Journal of Research in Science and Engineering (JRSE)
ISSN: 1656-1996 Volume-6, Issue-12, December 2024
DOI: 10.53469/jrse.2024.06(12).11

Research on Land Subsidence Prediction in Mining Areas Based on SBAS-InSAR and Multi-Model Comparison

Qingkun Yang[1], Peihua Xu[1], Chen Cao[2], Bo Shan[2], Yimin Liu[2], Tie Jin[3], Xiguan An[3]

[1]College of Construction Engineering, Jilin University, Changchun 130012, Jilin, China
[2]Northeast Electric Power Design Institute, Changchun 130021, Jilin, China
[3]Geological Survey Academy of Inner Mongolia Autonomous Region, Hohhot 010020, Inner Mongolia, China

Abstract: ***Land subsidence in mining areas caused by underground resource exploitation poses a serious threat to surface stability and ecological security. Accurate prediction of land subsidence is crucial for disaster prevention and mitigation in mining areas. This study integrates SBAS-InSAR technology with various predictive models to analyze and forecast surface subsidence in mining areas. First, SBAS-InSAR technology is used to process Sentinel-1 data from 2018 to 2023, extracting time-series deformation data in the study area. Then, based on the key influencing factors of land subsidence, a comparative analysis of multiple models, including SVR, PSO-SVR, and HOLT, is conducted to assess their performance in subsidence prediction. The results show that the PSO-SVR model, optimized with particle swarm optimization, demonstrates superior accuracy and reliability compared to the other models. This provides a robust approach for monitoring and predicting land subsidence in mining areas, offering technical support for risk management and sustainable resource development.***

Keywords: Mining Areas, Land Subsidence, Multi-Model Comparison, PSO-SVR, Prediction Analysis.

1. Introduction

Land subsidence caused by underground resource exploitation is a common geological disaster in mining areas. It not only affects surface stability but also poses a significant threat to ecological safety and the normal operation of infrastructure. Accurate prediction of land subsidence is of great importance for disaster prevention, mitigation, and the sustainable development of mining areas.

In recent years, remote sensing technology has provided new tools and methods for monitoring land subsidence. Among these, SBAS-InSAR (Small Baseline Subset Interferometric Synthetic Aperture Radar) technology has gained attention for its ability to monitor large-scale surface deformation with high accuracy and temporal resolution. SBAS-InSAR can effectively capture subsidence information over time and has been widely applied in mining areas. However, the accuracy and reliability of subsidence predictions still depend on the performance of predictive models and the integration of key influencing factors.

A mining-induced subsidence area refers to a geological impact zone formed as a result of mineral resource extraction activities. Surface deformation in this area is primarily caused by the extraction of underground coal seams or mineral deposits, leading to the release of strata stress, the formation of underground voids, and subsequent surface subsidence and deformation. Characteristics of mining-induced subsidence areas include significant spatial and temporal heterogeneity in surface deformation, which exhibits cumulative or abrupt patterns depending on the depth, extent, and duration of mining activities. Since these areas are influenced by both natural conditions (e.g., geological structures, rainfall) and human activities (e.g., mining methods, land use), the occurrence of surface subsidence is often complex and diverse. Accurate monitoring and scientific modeling are required for effective prediction and management.

Existing predictive models, such as statistical methods, machine learning approaches, and time-series models, have demonstrated certain advantages in subsidence prediction. However, these models also have limitations in dealing with complex geological conditions and nonlinear relationships among influencing factors. To address these challenges, this study integrates SBAS-InSAR technology with multiple predictive models, including SVR (Support Vector Regression), PSO-SVR (Particle Swarm Optimization Support Vector Regression), and HOLT (Holt's Exponential Smoothing), to analyze and predict land subsidence in mining areas. By comparing the performance of these models, this study aims to provide an accurate and efficient method for subsidence prediction, offering a reference for disaster prevention and management in mining areas.

2. Overview of the Study Area

The study area is located in Baishui County, Shaanxi Province, which is part of the Loess Plateau and features significant mining activity with complex geological conditions. The terrain is primarily hilly, with the typical characteristics of the Loess Plateau, including thick loess deposits and steep slopes. Land subsidence is a common phenomenon in this area due to extensive underground coal mining.

The region experiences a semi-arid continental climate, with an annual average precipitation of approximately 500 mm, most of which is concentrated during the summer months. The geological structure is dominated by thick loess layers interspersed with sedimentary rock formations, which are highly prone to deformation under external factors such as mining activities or heavy rainfall infiltration.

The mining activities in the area have altered the subsurface structure, creating voids that lead to surface instability and increased the risk of land subsidence. These conditions

necessitate effective monitoring and predictive modeling to mitigate potential hazards and ensure the safety of local infrastructure and communities.

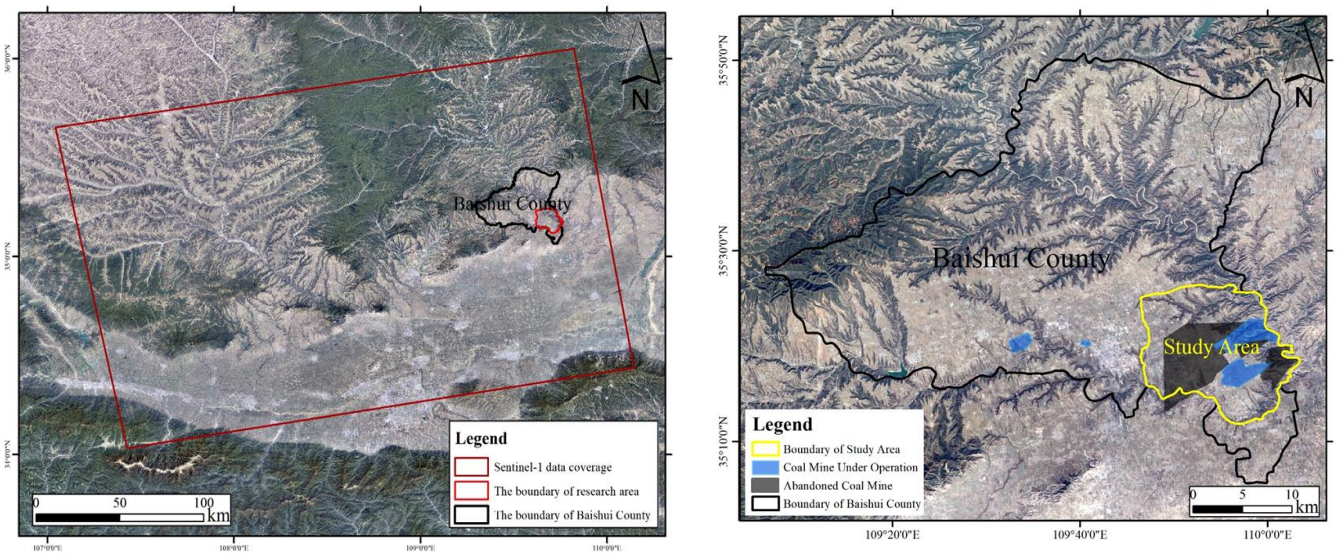

(a) Study Area and Sentinel-1 Data Coverage

(b) Detailed Study Area in Baishui County

Figure 1: Research Area and Data Extent Maps

3. Research Methods

This study integrates multiple data processing and analysis methods to improve the accuracy and reliability of land subsidence prediction. High-precision surface deformation data were obtained using SBAS-InSAR technology, and the data were processed to remove outliers and perform interpolation, ensuring completeness and accuracy. To further analyze the influencing factors of land subsidence, an information entropy model was employed to identify the most significant factors. Subsequently, gray relational analysis and principal component analysis were utilized to reduce the dimensionality of the influencing factors, thereby minimizing data redundancy and enhancing computational efficiency. Based on this, the processed data were input into the PSO-SVR model, where particle swarm optimization was applied to optimize the parameters of the support vector regression model. This approach enabled accurate prediction of land subsidence, ensuring optimal data quality and computational performance of the predictive model.

3.1 Data Preprocessing

3.1.1 Abnormal data removal

Gross error refers to abnormal errors or outliers in InSAR data processing, which may be caused by atmospheric delay, orbit error and surface scattering change [8]. Gross error detection and elimination are carried out by setting sliding window. Gross error is defined as the observed value of the local conversion median absolute deviation (SMAD) that is more than three times the difference from the local median in the sliding window [9], and the SMAD calculation method is shown in Equation 1.

$$SMAD = C \cdot median(|S_i - median(S)|), C = -1/(sqrt(2) \cdot erfcinv(3/2)) \quad (1)$$

3.1.2 Gaussian interpolation

In time series forecasting, insufficient data may lead to overfitting of the model. Compared with sufficient data, insufficient data may also lead to overfitting of the model to the existing data [10], thus reducing the generalization ability of the model and reducing the reliability of the predicted shape variables in practical applications. Insufficient data may also lead to difficulty in feature extraction and information loss in the extraction process [11].

The Gaussian interpolation algorithm approximates the time series deformation data as Gaussian distribution by combining prior information, and uses the maximum amplitude of the shape variable and the sub-maximum value corresponding to the left and right of the distance unit for interpolation operation processing [12]. Let the probability density function of the Gaussian distribution be:

$$f(t) = \frac{1}{\sqrt{2\pi\sigma^2}} exp(-\frac{(t-t_0)^2}{2\sigma^2}) \quad (2)$$

Where, t0 represents the mean of the Gaussian distribution and σ2 represents the variance of the Gaussian distribution.

3.2 Information Content Model

The information content model is a statistical prediction method derived from the information content, which can better reflect the contribution rate of different classification intervals of various impact factors to the land surface settlement [13]. The information content can quantitatively represent the characteristics of land subsidence prone places, and the prediction points can be selected by comprehensive use of the information analysis results and the SBAS-InSAR processing results [14]. The calculation formula of the information content model is shown in equation (3).

$$I = \ln \frac{N_i/N}{S_i/S} \quad (3)$$

Where: I information amount of serious surface deformation in section i of factor A; Ni represents the number of grids with severe surface deformation in the i section of the influence factor A. N represents the total number of grids with severe surface deformation in the study area. Si represents the

number of grids in the i interval of the influence factor A; S represents the total number of grids in the study area.

3.3 Grey Correlation Analysis

Grey correlation analysis uses grey correlation degree to quantitatively describe the closeness of the connection between various factors [15]. In this study, grey correlation analysis was used to initially screen the factors closely related to the land surface settlement. (1) Determine the reference sequence, k=1,2,...,n and comparison sequence, k=1,2,... n, i=1,2,...,m, where n corresponds to the number of time periods, and m is the number of corresponding columns of the comparison sequence. (2) Dimensionless processing, in order to reduce the error caused by dimensionality, the data is processed by means of averaging; (3) Calculate the grey correlation coefficient. The maximum and minimum of the absolute difference between the reference sequence and the comparison sequence are solved, and the grey correlation coefficient is calculated according to equation (3). (4) Calculate the grey correlation degree.

$$\varepsilon_i(k) = \frac{\min_i \min_k |Y(k) - X_i(k)| + \rho \max_i \max_k |Y(k) - X_i(k)|}{|Y(k) - X_i(k)| + \rho \max_i \max_k |Y(k) - X_i(k)|} \quad (4)$$

3.4 Principal Component Analysis

Principal component analysis is a commonly used data analysis and processing method, which uses orthogonal transformation to transform a set of related data into a set of data that is linearly independent in all dimensions to achieve the purpose of extracting principal components [16]. In this study, the partial correlation coefficient between the influencing factors was calculated using the KMO test method [17], and after determining that the correlation between the influencing factors was strong, the principal component analysis method was used for data dimensionality reduction. (1) In order to avoid the influence caused by dimension, the original data is standardized to obtain A new matrix A; (2) Calculate the covariance matrix C of matrix A, the eigenvalues of matrix C and the corresponding eigenvectors; (3) The original feature is projected onto the selected feature vector to obtain the new K-dimensional feature after dimensionality reduction; (4) Select all principal components whose cumulative contribution rate is greater than 90% and calculate the principal component expression.

Place table titles above the tables.

3.5Holt Model

Holt model is a kind of time series prediction model, which is often used to predict time series data with trend changes. It is an extension of exponential smoothing model. The Holt model processes the level and trend of data through two smoothing equations, and is suitable for time series with obvious trend [18].

$$S_t = \alpha X_t + (1-\alpha)(S_{t-1} + T_{t-1}) \quad (5)$$

$$T_t = \gamma(S_t - S_{t-1}) + (1-\gamma)T_{t-1} \quad (6)$$

$$X_{t+m} = S_t + mT_t \quad (7)$$

In the formula, St and ST-1 respectively represent the estimation of the trend of the t period or the T-1 period using the data of the pre-T period and the pre-T-1 period, Tt and TT-1 respectively represent the estimation of the trend increment using the data of the pre-T period or the pre-T-1 period, α and γ are smoothing parameters, $0 \le \alpha \le 1, 0 \le \gamma \le 1$, Xt is the actual observed value of the t period. Xt +m is the predicted value of the t+m period, and m is the number of predicted extrapolations.

3.6 PSO-SVR Model

The prediction accuracy of SVR model is affected by penalty coefficient (C) and kernel function parameter (g), and the prediction results are different with different hyperparameter Settings [19].

In order to improve the prediction accuracy, modeling efficiency and generalization ability of SVR model, many scholars at home and abroad have studied the parameter optimization of SVR model, but no universally recognized and unified optimization method has been established so far. Common optimization methods include grid search, genetic algorithm, particle swarm optimization, etc. [20-23]. particle swarm optimization (PSO) has the advantages of fast convergence speed, high computational efficiency, and effective solution of local optimal solutions [24-26], so this study uses PSO algorithm for hyperparameter optimization. The PSO algorithm determines the fitness function by initializing the number of particles and the initial position and velocity of each particle. At the same time, in order to avoid the occurrence of local optimal solutions, nonlinear decreasing inertia weights and compression factors are used to search from global to local, and the local and global optimal locations of particles are iteratively updated constantly, the optimal locations in the entire particle swarm are evaluated and selected, and the optimal penalty coefficient (C) and kernel function parameter (g) are found [26].

4. Surface Subsidence Analysis Based on SBAS-InSAR

This study utilized SBAS-InSAR technology to process 70 scenes of synthetic aperture radar (SAR) images.

(1) The orbital information of the single-look complex (SLC) images was corrected using precise orbit data, and the original SAR images were cropped to extract the study area; (2) Based on the criteria of a spatial baseline within 2% of the critical baseline and a temporal baseline of 120 days, 117 interferometric pairs were constructed (as shown in Figure 2); (3) The SAR image from February 4, 2018, was selected as the master image according to the temporal baseline and minimum principles. All slave images were coregistered to the master image. Complex interferograms were generated by conjugate multiplying the complex images of each interferometric pair, and flat-earth and topographic phases were removed using precise orbital data and external DEMs; (4) The minimum cost flow method was used for phase unwrapping; (5) SBAS inversion estimation and geocoding were performed to obtain time-series deformation maps along the line of sight (LOS) in the WGS84 coordinate system; (6) Gross error detection and removal were conducted using a sliding window approach. The filtered data were then interpolated using Gaussian interpolation to generate the

deformation velocity raster of the study area.

The surface deformation velocity results of the study area are shown in Figure 3. Significant spatial differences in ground subsidence can be observed across the study area, primarily concentrated in coal mining regions. In particular, the contrast in deformation rates between active mining areas and ceased mining areas reveals the impact of different mining activities on surface stability. High subsidence velocity areas are mainly concentrated near the Xigu Xinxing Coal Mine and the Pubaixigu Coal Mine, indicating that mining activities in these areas have caused significant ground subsidence. These high subsidence rates are closely associated with mining-induced zones beneath the surface, likely caused by underground voids formed after coal seam extraction and the release of strata stress. Moderate subsidence velocity areas are mostly distributed along the edges of mining zones or in regions affected by mining activities. This suggests that mining activities have an impact on surrounding areas, although the degree of ground subsidence is relatively minor.

In ceased mining areas, subsidence rates are generally low, indicating that the trend of ground subsidence has mitigated after mining activities ceased. However, in areas where mining activities continue, particularly along the boundary regions of the Xigu Xinxing Coal Mine, subsidence rates remain high, suggesting that ongoing mining activities are still exacerbating surface subsidence.

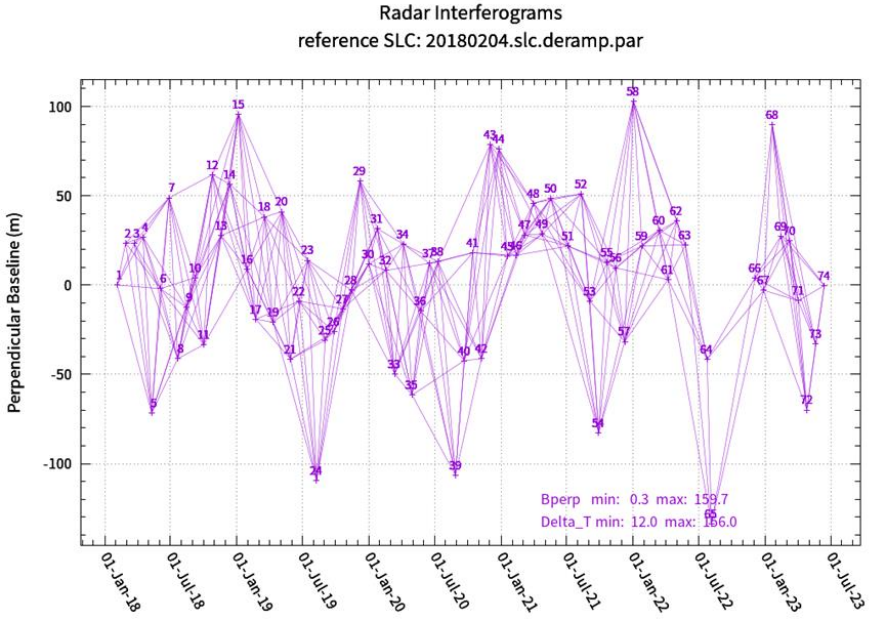

Figure 2: The temporal baseline chart

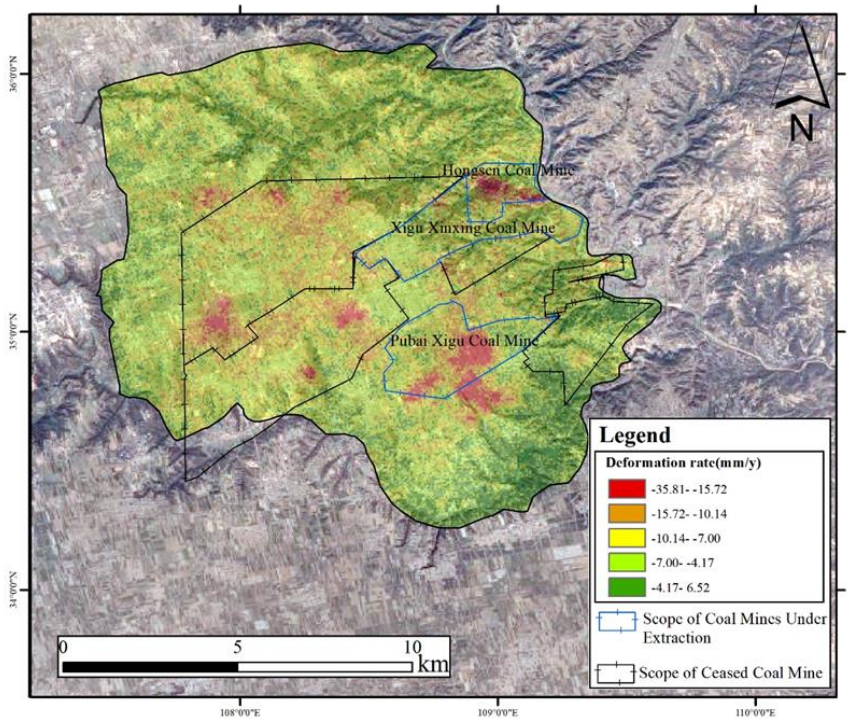

Figure 3: Distribution Map of Land Subsidence Deformation Rate and Coal Mining Status in Mining Area

5. Other Recommendations

5.1 Selection of Feature Points Based on the Information Entropy Model

In analyzing the influencing factors of surface deformation in the study area, a variety of factors were considered, primarily categorized into natural geological factors and human activity factors. Natural geological factors include lithology, terrain relief, groundwater level changes, and distance to rivers, which mainly reflect the natural driving forces of geological conditions and the hydrological environment on surface deformation. Human activity factors include land use type, distance to roads, and the distribution of mining areas, which represent the impact of human development activities on surface stability. Among these factors, this study ultimately selected annual precipitation, land use type, distance to roads, lithology, and terrain relief as the primary research variables. Precipitation serves as a critical external factor that reduces the mechanical properties of rock and soil, leading to deformation. Land use type reveals the diverse impacts of different human activities on the surface. Distance to roads reflects the dynamic influence of traffic loads on the surface. Lithology determines the bearing capacity and stability of soil layers, while terrain relief helps identify deformation risks in high-slope areas. The selection of these factors is based on a comprehensive consideration of natural and human driving mechanisms, ensuring the precision and comprehensiveness of the predictive model.

Land use type, terrain relief, distance to roads, lithology, and rainfall are the primary factors influencing surface deformation. Land use type is categorized into grassland, cropland, forest, water bodies, bare land, and artificial surfaces, reflecting the varied impacts of human activities on surface stability. Lithology illustrates the stability differences of various rock and soil materials under geological stress, with these two factors classified according to the categories in the collected data. Terrain relief is used to evaluate the impact of geomorphological features on subsidence, distance to roads is analyzed through buffer zones to reveal the compressive effects of traffic loads on the surface, and rainfall reflects the spatiotemporal correlation between precipitation and subsidence. These four factors are classified using the natural breaks method. The categorization and selection of these factors comprehensively consider the dual driving mechanisms of natural conditions and human activities on surface deformation.

Based on the classification of the five identified influencing factors, the spatial distribution of severe surface subsidence was statistically analyzed using Equation (3).

Table 1: Calculation Results of Information Content for Static Influencing Factors

Impact factor	The impact factor classification information	The amount of impact factor
Topographic relief	452.40-537.61	0.10
	537.61-614.96	0.31
	614.96-668.70	0.36
	668.70-721.14	0.21
	721.14-788	-0.06
Land use type	Grassland	0.11
	Arable land	0.47
	Water body	-0.23
	Woodland	0.01
	Artificial surface	-0.15
	Bare ground	0.04
Distance from road	<50m	0.02
	50-100m	0.08
	100-200m	0.16
	>200m	0.54
The stratum lithology	The carboniferous Taiyuan Formation shale, sandstone and limestone with coal seam	-0.13
	Permian Shihezi Formation shale and quartz sandstone with coal seam	0.06
	Sandstone and sandy shale of Permian Shiqianfeng Formation	0.02
	Quaternary Holocene subsandy soil, silty soil, sand gravel	0.01
	Quaternary Pleistocene loess	0.82
	Quaternary Pleistocene loess-like subclay and sand-gravel strata	-0.01
	Ordovician Majiagou Series upper thin layer limestone and chert limestone	-5.68
	Quaternary Pleistocene loess and paleosoil layer	0.08
	Unidentified geologic body	-1.87
Rainfall	4679.7-4786.9	0.06
	4786.9-4861.3	0.13
	4961.3-4925.4	0.18
	4925.4-4994.5	0.15
	4994.5-5120.8	0.21

The larger the information entropy, the higher the likelihood of severe land subsidence in the area. According to Table 1, surface subsidence in the study area is more commonly observed in locations where annual rainfall ranges from 4994.5 to 5120.8 mm, terrain relief is between 614.96 and 668.70, the land use type is cropland, the distance to roads is >200 m, and the lithology is Quaternary loess of the Pleistocene series. Combining the terrain characteristics of areas prone to land subsidence and the surface deformation results obtained using SBAS-InSAR technology, Feature Point 1 and Feature Point 2 were selected from coherent points in the study area for prediction. Their specific locations are shown in Figure 4.

5.2 Influencing Factor Correlation and Principal Component Analysis

A gray relational analysis was conducted on the five proposed influencing factors and the subsidence volume. The average gray relational degree between the five influencing factors and the cumulative subsidence volume of coherent points in the study area was calculated, as shown in Table 2. The results indicate that terrain relief, land use type, distance to roads, and lithology all have a gray relational degree greater than 0.6 with the surface subsidence volume. Therefore, these four influencing factors are closely related to the subsidence volume and were selected as the key influencing factors for further analysis.

Table 2: Factor Association and Correlation Table

Influencing Factors	Terrain Relief	Land Use Type	Distance to Roads	Lithology	Annual Average Rainfall
Gray Relational Degree	0.6559	0.7593	0.7165	0.6314	0.3428
KMO	0.8536	0.8769	0.8242	0.8397	0.5113

Among the various factors influencing surface deformation, key influencing factors were identified through gray relational analysis and KMO testing, and their relational degrees and

correlations were calculated, as shown in Table 2. Terrain relief, land use type, distance to roads, and lithology all have relatively high gray relational degrees with surface subsidence, indicating a close relationship between these factors and surface subsidence. To further analyze the classification of different influencing factors, Figure 5 illustrates the specific spatial distribution of each factor.

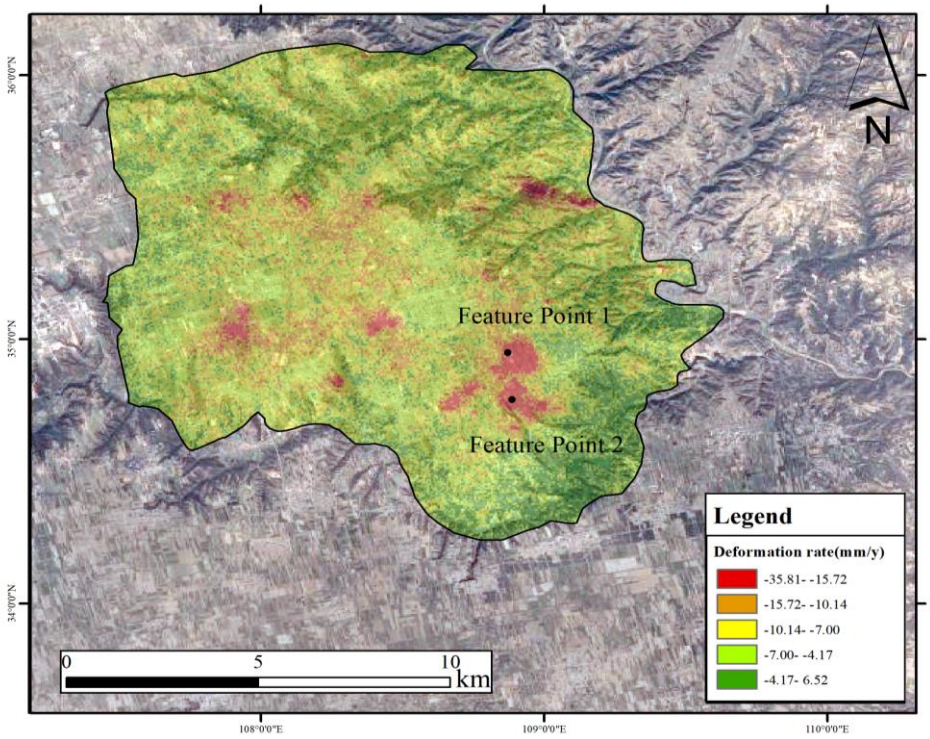

Figure 4: Location Map of feature points

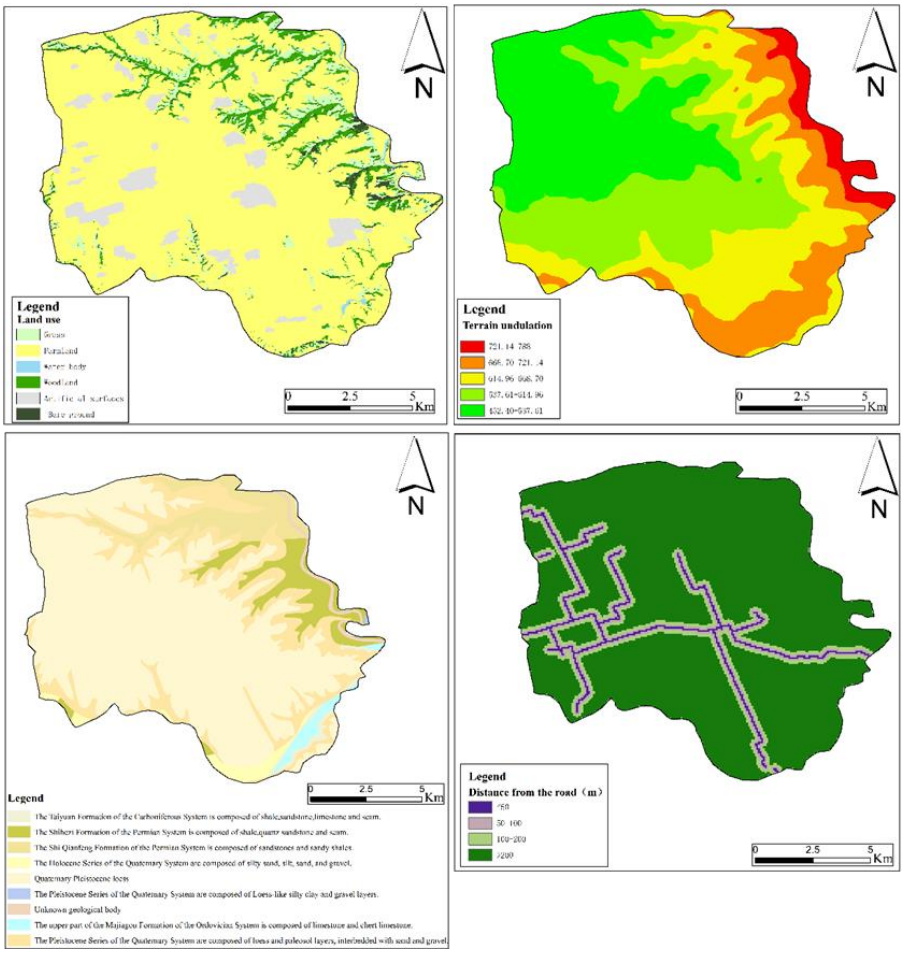

Figure 5: Figure of Influencing Factors Classification: (a) Land Use Type; (b) Terrain Relief; (c) Lithology; (d) Distance from Roads

The KMO test method was used to examine the correlation among the four influencing factors, and the KMO test value was found to be greater than 0.8, indicating a strong correlation among the four factors, making them suitable for factor analysis. However, directly inputting these factors into the prediction model may lead to overfitting. Principal Component Analysis (PCA) is a commonly used data dimensionality reduction method that transforms original variables into linearly independent principal components through linear transformations, thereby reducing data dimensions and avoiding multicollinearity issues.

In this study, PCA was applied to the four high gray relational degree factors: terrain relief, land use type, distance to roads, and lithology. First, the data were standardized to eliminate dimensional differences. Then, the covariance matrix was calculated, and eigenvalues and eigenvectors were extracted. Finally, three principal components with a cumulative variance contribution rate greater than 90% were selected (see Equation 8).These three principal components comprehensively reflect the main influencing factors of land subsidence in mining areas from the perspectives of terrain characteristics, human activities, and geological structures. The first principal component reveals the natural driving effects of geomorphological conditions on subsidence; the second principal component emphasizes the accelerating effects of human activities on surface deformation; and the third principal component focuses on the mechanical response characteristics of rock and soil materials. The extraction and application of these three principal components not only simplify the dimensionality of the factors but also provide a clear theoretical basis for land subsidence prediction.

$$\begin{aligned} y_1 &= -0.27x_1 - 0.41x_2 + 0.46x_3 + 0.52x_4 \\ y_2 &= 0.46x_1 - 0.54x_2 - 0.04x_3 + 0.13x_4 \\ y_3 &= 0.38x_1 + 0.24x_2 + 0.73x_3 - 0.18x_4 \end{aligned} \quad (8)$$

6. Multi-Model Comparison for Subsidence Trend Prediction

6.1 Data Preprocessing

This study used the particle swarm optimization (PSO) algorithm to optimize the penalty coefficient (C) and kernel function parameter (g) of the SVR model, constructing a PSO-SVR prediction model. The LOS subsidence data of Feature Point 1 and Feature Point 2 from Figure 4, along with the three principal components (Equation 8), were used as datasets. The datasets were divided into a training set (90%) and a test set (10%). The root mean square error (RMSE) between the test set and the predicted values was used as the fitness function. The optimization range for the penalty coefficient (C) and kernel function parameter (g) was set to [0,100] and [0,1], respectively. The identified hyperparameters were input into the PSO-SVR model for prediction, and the results are shown in Figure 6.

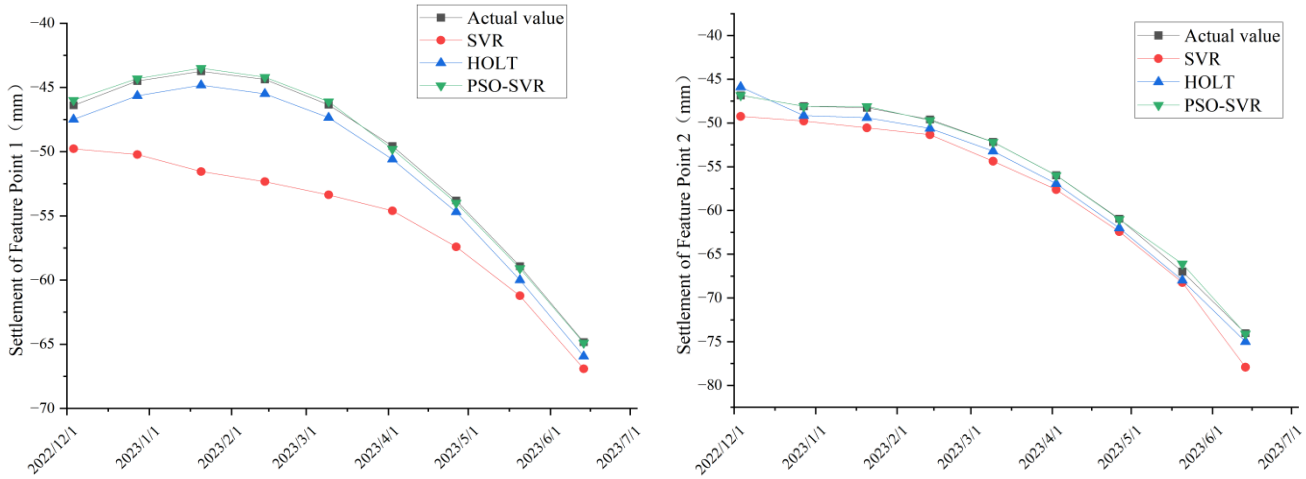

Figure 6: The prediction results of different model for each deformation points

As shown in Figure 6, land subsidence in the mining area exhibits a cumulative trend that increases progressively over time, with deformation magnitude continuously intensifying and showing no signs of stabilization. Additionally, the subsidence rate accelerates in the later stages, reflecting the gradual transmission of subsurface strata instability to the surface in the mining area.

When seasonal ground deformation rebound phenomena occur due to rainfall variations, the SVR model shows weak predictive capability for these phenomena. The prediction curve for Feature Point 2 indicates that the model's performance improves when the subsidence trend is relatively consistent. The Holt model demonstrates relatively stable performance, closely aligning with the actual subsidence trend throughout the time period. However, it shows slight deviations at the initial and final stages, with its performance potentially inversely related to the prediction period length. The PSO-SVR model exhibits a high degree of fit with the actual values, particularly at the initial and final stages, where its prediction accuracy surpasses that of the Holt and SVR models, with smaller errors. During the rapid decline phase of the subsidence rate at Feature Point 2, the PSO-SVR model captures the changes more accurately than the Holt and SVR models.

The PSO-SVR model demonstrates high predictive accuracy and stability in both simulations, particularly under complex nonlinear trends. It exhibits superior capability in capturing subsidence variations, highlighting its advantages in such scenarios.

6.2 Multi-model Accuracy Analysis

As shown in Figure 6, the prediction results of the PSO-SVR model are closer to the deformation data obtained using SBAS-InSAR technology. The mean squared error (MSE), root mean squared error (RMSE), mean absolute error (MAE), and coefficient of determination (R^2) between the test set and the two groups of prediction results were calculated, and the results are presented in Figure 7.

In terms of error metrics, the PSO-SVR model exhibits the smallest errors. Across the two figures, the PSO-SVR model outperforms the SVR and Holt models with lower values in MSE, RMSE, and MAE, indicating that the predictions made by the PSO-SVR model are more accurate. Regarding goodness of fit, the PSO-SVR model also surpasses the other two models, demonstrating its superior ability to fit ground subsidence data and capture more precise trends.

Comparatively, the PSO-SVR model achieves better performance than the Holt model across all error evaluation metrics, resulting in more accurate predictions. These results confirm the reliability of the PSO-SVR model in predicting surface subsidence in mining areas. The model effectively avoids overfitting issues, enhancing its generalization ability and predictive performance.

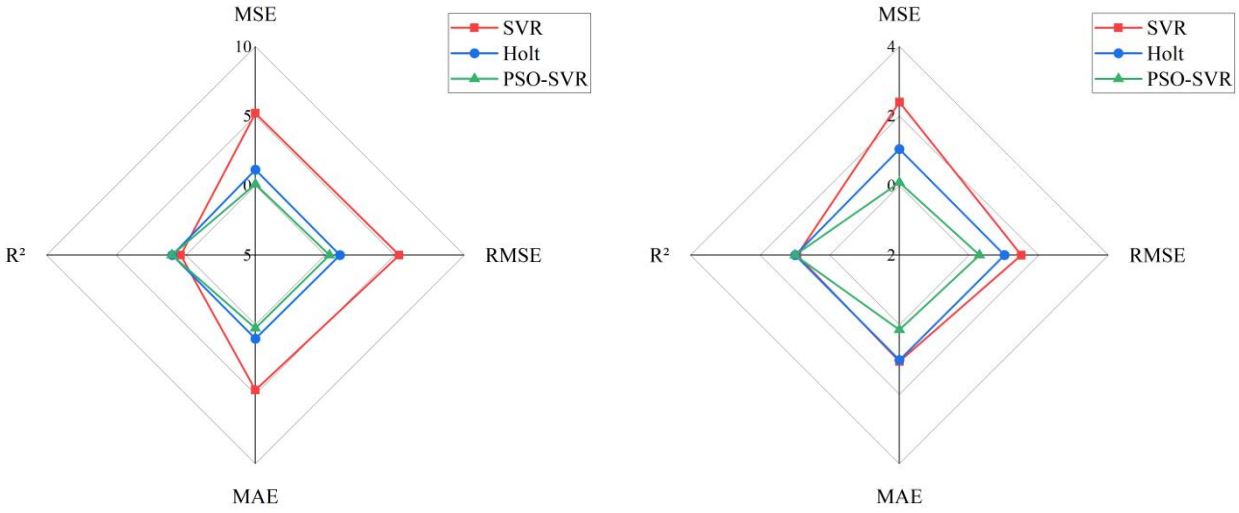

Figure 7: Comparison of Prediction Performance Metrics across Different Models

7. Conclusion

In this study, three time-series prediction models, namely SVR, Holt, and PSO-SVR, were used. Based on SBAS-InSAR surface deformation data, time-series prediction of progressive and abrupt surface deformation in the mining areas of Leiya Township and Xigu Town in southeastern Baishui County was conducted. The following conclusions were drawn:

(1) By removing outliers and applying Gaussian interpolation, high-precision deformation data were obtained using SBAS-InSAR technology. This provides a reference for monitoring deformation in mining areas and establishes a reliable dataset for subsequent prediction efforts.

(2) The spatial distribution of severe surface subsidence areas was statistically analyzed using the information entropy model, allowing for an understanding of the terrain characteristics in regions prone to surface subsidence. Influencing factors closely related to surface deformation were analyzed through gray relational analysis and principal component analysis.

(3) Surface subsidence was predicted using the PSO-SVR model, along with SVR and Holt models. The results show that the prediction accuracy of the PSO-SVR model is superior to that of the SVR and Holt models, with the PSO-SVR model achieving the smallest error when compared to the test set. Additionally, it demonstrated greater sensitivity to changes in trends. Therefore, the PSO-SVR model proves to have strong practicality in predicting surface subsidence in mining areas.

References

[1] CHAUSSARD E, WDOWINSKI S, CABRAL-CANO E, et al. Land subsidence in central Mexico detected by ALOS InSAR time-series [J]. Remote Sens Environ, 2014, 140: 94-106.

[2] WU Z R, MA P F, ZHENG Y, et al. Automatic detection and classification of land subsidence in deltaic metropolitan areas using distributed scatterer InSAR and Oriented R-CNN [J]. Remote Sens Environ, 2023, 290: 19.

[3] OSMANOGLU B, SUNAR F, WDOWINSKI S, et al. Time series analysis of InSAR data: Methods and trends [J]. ISPRS-J Photogramm Remote Sens, 2016, 115: 90-102.

[4] ROSI A, TOFANI V, TANTERI L, et al. The new landslide inventory of Tuscany (Italy) updated with PS-InSAR: geomorphological features and landslide distribution [J]. Landslides, 2018, 15(1): 5-19.

[5] KULIBABA S B. INFLUENCE OF THE MULTIPLICITY OF THE EARTH'S SURFACE UNDERMINING ON THE VALUE OF THE SUBSIDENCE ANGLE [J]. Proc Tula States Univ-Sci Earth, 2022, 4: 264-73.

[6] GONG X L, GENG J S, SUN Q, et al. Experimental study on pumping-induced land subsidence and earth

fissures: a case study in the Su-Xi-Chang region, China [J]. Bull Eng Geol Environ, 2020, 79(9): 4515-25.

[7] LI P, WANG J, LIU M M, et al. Spatio-temporal variation characteristics of NDVI and its response to climate on the Loess Plateau from 1985 to 2015 [J]. Catena, 2021, 203: 11.

[8] CUI J W, CHEN X W, HAN W T, et al. Estimation of Soil Salt Content at Different Depths Using UAV Multi-Spectral Remote Sensing Combined with Machine Learning Algorithms [J]. Remote Sens, 2023, 15(21): 20.

[9] ZHANG L L, DAI K R, DENG J, et al. Identifying Potential Landslides by Stacking-InSAR in Southwestern China and Its Performance Comparison with SBAS-InSAR [J]. Remote Sens, 2021, 13(18): 14.

[10] MA P F, YU C, JIAO Z Y, et al. Improving time-series InSAR deformation estimation for city clusters by deep learning-based atmospheric delay correction [J]. Remote Sens Environ, 2024, 304: 15.

[11] ZHOU C, CAO Y, HU X, et al. Enhanced dynamic landslide hazard mapping using MT-InSAR method in the Three Gorges Reservoir Area [J]. Landslides, 2022, 19(7): 1585-97.

[12] LAN Y, YU H W, XING M D, et al. AN INFINITY-NORM-BASED PHASE UNWRAPPING METHOD WITH TSPA FRAMEWORK FOR MULTI-BASELINE SAR INTERFEROGRAMS; proceedings of the IEEE International Geoscience and Remote Sensing Symposium (IGARSS), Electr Network, F Sep 26-Oct 02, 2020 [C]. Ieee: NEW YORK, 2020.

[13] LENG J, GAO M L, GONG H L, et al. Spatio-temporal prediction of regional land subsidence via ConvLSTM [J]. J Geogr Sci, 2023, 33(10): 2131-56.

[14] LI F K, LIU G L, TAO Q X, et al. Land subsidence prediction model based on its influencing factors and machine learning methods [J]. Nat Hazards, 2023, 116(3): 3015-41.

[15] XIE Z W, HU H H. Improved grey prediction model for land subsidence at finished underground mining; proceedings of the International Conference on Mine Hazards Prevention and Control, Qingdao, PEOPLES R CHINA, F Oct 17, 2007 [C]. Science Press Beijing: BEIJING, 2007.

[16] ZHOU D Y, ZUO X Q, ZHAO Z F. Constructing a Large-Scale Urban Land Subsidence Prediction Method Based on Neural Network Algorithm from the Perspective of Multiple Factors [J]. Remote Sens, 2022, 14(8): 32.

[17] XIE Z W, HU H H, LI S Q, et al. GM-SVM prediction model for land subsidence at finished underground mining and its application; proceedings of the 3rd International Symposium on Modern Mining and Safety Technology, Liaoning Tech Univ, Fuxin, PEOPLES R CHINA, F Aug 04-06, 2008 [C]. Coal Industry Publ House: BEIJING, 2008.

[18] HE Y, YAN H W, YANG W, et al. Time-Series Analysis and Prediction of Surface Deformation in the Jinchuan Mining Area, Gansu Province, by Using InSAR and CNN-PhLSTM Network [J]. IEEE J Sel Top Appl Earth Observ Remote Sens, 2022, 15: 6732-51.

[19] LI L, WU K, ZHOU D W. Extraction algorithm of mining subsidence information on water area based on support vector machine [J]. Environ Earth Sci, 2014, 72(10): 3991-4000.

[20] ZEYDALINEJAD N, DEHGHANI R. Use of meta-heuristic approach in the estimation of aquifer?s response to climate change under shared socioeconomic pathways [J]. Groundwater Sustain Dev, 2023, 20: 25.

[21] ZHANG L, ARABAMERI A, SANTOSH M, et al. Land subsidence susceptibility mapping: comparative assessment of the efficacy of the five models [J]. Environ Sci Pollut Res, 2023, 30(31): 77830-49.

[22] MA F, SUI L C, LIAN W. Prediction of Mine Subsidence Based on InSAR Technology and the LSTM Algorithm: A Case Study of the Shigouyi Coalfield, Ningxia (China) [J]. Remote Sens, 2023, 15(11): 22.

[23] LYU M, LI X J, KE Y H, et al. Reconstruction of spatially continuous time-series land subsidence based on PS-InSAR and improved MLS-SVR in Beijing Plain area [J]. GISci Remote Sens, 2023, 60(1): 22.

[24] AMR D, DING X L, FEKRY R. A machine learning-based method for multi-satellite SAR data integration [J]. Egypt J Remote Sens Space Sci, 2024, 27(1): 1-9.

[25] SUI L C, MA F, CHEN N. Mining Subsidence Prediction by Combining Support Vector Machine Regression and Interferometric Synthetic Aperture Radar Data [J]. ISPRS Int Geo-Inf, 2020, 9(6): 17.

[26] TRIPATHI A, MALIK K, RESHI A R, et al. Multi-temporal SAR Interferometry (MTInSAR)-based study of surface subsidence and its impact on Krishna Godavari (KG) basin in India: a support vector approach [J]. Environ Monit Assess, 2023, 195(11): 17.

[27] HAKIM W L, FADHILLAH M F, PARK S, et al. InSAR time-series analysis and susceptibility mapping for land subsidence in Semarang, Indonesia using convolutional neural network and support vector regression [J]. Remote Sens Environ, 2023, 287: 16.